Check for updates

ChemPlusChem

Research Article
doi.org/10.1002/cplu.202400055

Chemistry Europe
European Chemical Societies Publishing

www.chempluschem.org

Competitive Intramolecular Hydrogen Bonding: Offering Molecules a Choice

Yu Sun,[a] Evelyn R. Morton,[a] Hunaida Bhabha,[a] Ewan R. Clark,[b] Dejan-Krešimir Bučar,[a] Victoria Barros-Metlova,[a] Jamie A. Gould,[a] Abil E. Aliev,*[a] and Cally J. E. Haynes*[a]

The conformational preferences of *N*-((6-methylpyridin-2-yl)carbamothioyl)benzamide were studied in solution, the gas phase and the solid state via a combination of NMR, density functional theory (DFT) and single crystal X-ray techniques. This acyl thiourea derivative can adopt two classes of low energy conformation, each stabilized by a different 6-membered intramolecular hydrogen bond (IHB) pseudoring. Analysis in different solvents revealed that the conformational preference of this molecule is polarity dependent, with increasingly polar environments yielding a higher proportion of the minor conformer containing an NH···N IHB. The calculated barrier to interconversion is consistent with dynamic behaviour at room temperature, despite the propensity of 6-membered IHB pseudorings to be static. This work demonstrates that introducing competitive IHB pathways can render static IHBs more dynamic and that such systems could have potential as chameleons in drug design.

Introduction

Intramolecular hydrogen bond (IHB) formation is an important consideration in medicinal chemistry.[1] It can have a significant effect on the drug-like properties of small molecules, rigidifying their structure, affecting their binding to biological targets and shielding polar residues (increasing lipophilicity). A molecule that can reversibly convert between an "open" and a "closed" form can dynamically adapt its polar surface area (PSA). This provides an opportunity to maximise both water solubility and membrane permeability (Figure 1a), and such molecules are described as molecular chameleons due to their ability to change their appearance in response to their environment. This highly desirable effect can improve oral absorption,[2] and permeability across the blood-brain-barrier.[3] There is significant scope for IHB to aid the discovery and design of novel, orally available drugs based on large, flexible molecules in the beyond-Rule-of-5 (bRo5) chemical space.[4]

However, there is still limited understanding of how to design molecular chameleons.[5] In particular, if an IHB is static (not reversible) and the closed form dominates in any solvent/environment then chameleonic behaviour cannot be observed.[1a] Kuhn has catalogued the propensity of five- to eight-membered ring systems to form IHBs based on the prevalence of the IHB form in crystallographic databases.[1b] 6-membered IHB rings have a high propensity, which is significantly larger than 5, 7 and 8-membered rings and are

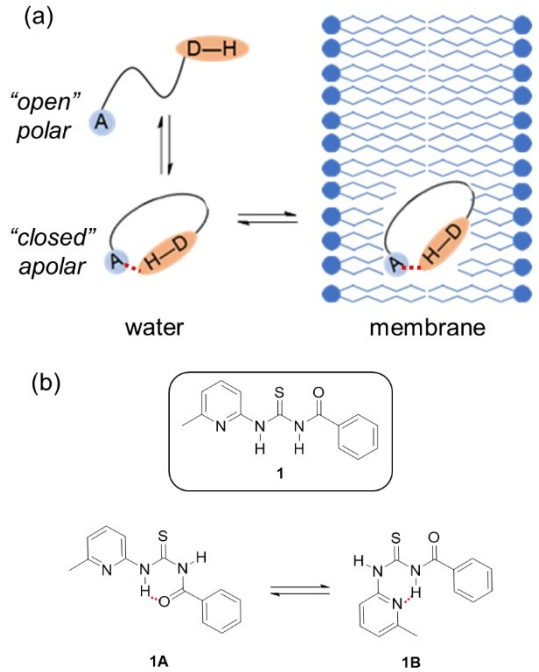

Figure 1. a) The transition between an "open" and "closed" forms of a molecular chameleon via the dynamic formation of an intramolecular hydrogen bond (IHB). A = hydrogen bond acceptor, D-H = hydrogen bond donor. The "open" form is polar and water soluble, while the apolar "closed" form is more lipophilic and membrane permeable; b) The structure of compound **1** (open form) and the two classes of IHB that could potentially be formed, giving closed forms **1 A** and **1 B**. Hydrogen bonds are shown as red dashed lines.

[a] *Y. Sun, E. R. Morton, H. Bhabha, Dr. D.-K. Bučar, V. Barros-Metlova, Dr. J. A. Gould, Dr. A. E. Aliev, Dr. C. J. E. Haynes*
Chemistry Department
University College London
20 Gordon Street, London WC1H 0AJ, UK
E-mail: A.E.Aliev@ucl.ac.uk
Cally.Haynes@ucl.ac.uk

[b] *Dr. E. R. Clark*
School of Chemistry and Forensics
University of Kent
Canterbury, CT2 7NH, UK

Supporting information for this article is available on the WWW under https://doi.org/10.1002/cplu.202400055

© 2024 The Authors. ChemPlusChem published by Wiley-VCH GmbH. This is an open access article under the terms of the Creative Commons Attribution License, which permits use, distribution and reproduction in any medium, provided the original work is properly cited.

© 2024 The Authors. ChemPlusChem published by Wiley-VCH GmbH

therefore often expected to be static. Previous studies of simple acyl thiourea derivatives have showed the presence of a 6-membered N–H···O IHB ring in the solid state and in solution.[6] Vidaluc and co-workers reported that the hydrogen bonded conformation of both aroyl(thio)urea and 2-pyridyl(thio)urea molecules crucially enhanced their acetylcholinesterase binding and inhibition activity.[7] Meanwhile, within the crystal engineering literature it is widely acknowledged that competition between supramolecular synthons (and the interactions they can form) can lead to polymorphism – in other words, the formation of multiple stable molecular arrangements in the solid state.[8] Fusco, Centore and colleagues have reported both tautomeric and conformational switching in a small molecule ligand in solution and the solid state in response to changes in protonation state and solvent polarity.[9] They also found that optimising intermolecular interactions was a key driving force for selection of tautomers of similar energy in the solid state.[10]

We speculated that a molecule with a choice of two stable IHB interactions may show dynamic behaviour as these two states may be closer in energy than typically considered "open" vs "closed" forms of a molecule. In this work we report investigations into the conformational preferences of N-((6-methylpyridin-2-yl)carbamothioyl)benzamide **1**. Highly similar structures have been reported as binders for the HIV-1 and hepatitis B capsid proteins, and thus are promising targets for antivirals.[11] Compound **1** is a small molecule which can form two different 6-membered IHB interactions containing either an O···H or N···H IHB (broadly grouped as **1 A** and **1 B**, Figure 1b). Using a combination of NMR, density functional theory (DFT) and single crystal X-ray techniques we established that **1** displays solvent polarity-dependent conformational preferences, indicating that this type of motif may switch its conformation in response to changes in environment. The energetic barrier to interconversion was determined via NMR and DFT approaches, providing evidence of dynamic exchange at room temperature under certain conditions.

Results and Discussion

NMR Analysis

Compound **1** was synthesised in one step via a modified literature procedure (SI Section S1).[12] Upon 1D ^{1}H NMR analysis in various solvents, we observed signals indicating the presence of both a major (assigned as **1 A**) and a minor species (**1 B**) in varying ratios (SI Section S2). In $CDCl_3$ the ratio between the major and minor conformers was approximately 20:1, measured using the integral intensities of well separated signals at 298 K (Figure S2). This ratio corresponds to 95% and 5% populations of conformers **1 A** and **1 B**, respectively, assuming a two-site exchange model. At 278 K in $CDCl_3$, the **1 A**-to-**1 B** ratio changes to approximately 17:1. Full spectral assignment via 1D and 2D NOE analysis revealed that **1 A** contained an N–H···O IHB and **1 B** contained an N–H···N hydrogen bond. In particular, significantly higher enhancements were observed for H9 in **1 B** (15.26 ppm, NOE 0.93%) compared to H9 in **1 A** (9.06 ppm, NOE 0.005%) with the methyl protons from C17 (Figure 2a). Similarly, an enhancement of 0.71% was observed at 8.09 ppm (1B H12,16) and 0.01% at 7.91 ppm (**1 B** H12,16) on selective inversion of Me protons in 1D NOESY experiments (Figure 2b). Based on the DFT-optimised geometries (see Section 3), the shortest distance from the Me carbon is 3.38 Å for H12,16 in **1 B** and 7.81 Å in **1 A**, which is in good agreement with the observed NOEs. As expected, the formation of a NH···O hydrogen bond in **1 A** led to a significant high frequency shift of +4.51 ppm for H7 (12.99 ppm) compared to H7 in **1 B** (8.48 ppm) at 298 K. Similarly, the NH···N hydrogen bond in **1 B** led to a significant high frequency shift of +6.12 ppm for H9 (15.15 ppm) compared to H9 in **1 A** (9.03 ppm) at 298 K.

The observed cross-peaks for proton H9 in **1 A** and proton H9 in **1 B** in the 2D NOESY spectrum confirmed the presence of a slow dynamic exchange on the NMR timescale (Figure S6, Supporting Information). A similar exchange effect was also confirmed by the 1D NOESY measurements (Figure S7, Supporting Information). Exchange cross-peaks for other proton pairs with relatively large chemical shift differences in **1 A** and **1 B** were also observed in the 2D NOESY spectrum (Figure S6, Supporting Information), confirming the presence of dynamic exchange between **1 A** and **1 B** in $CDCl_3$.

NMR spectra were also measured in CD_3COCD_3, CD_3CN and DMSO-d_6 in the temperature range 238–298 K (Tables S4–S6 in Supporting Information). The **1 A**-to-**1 B** conformer ratios

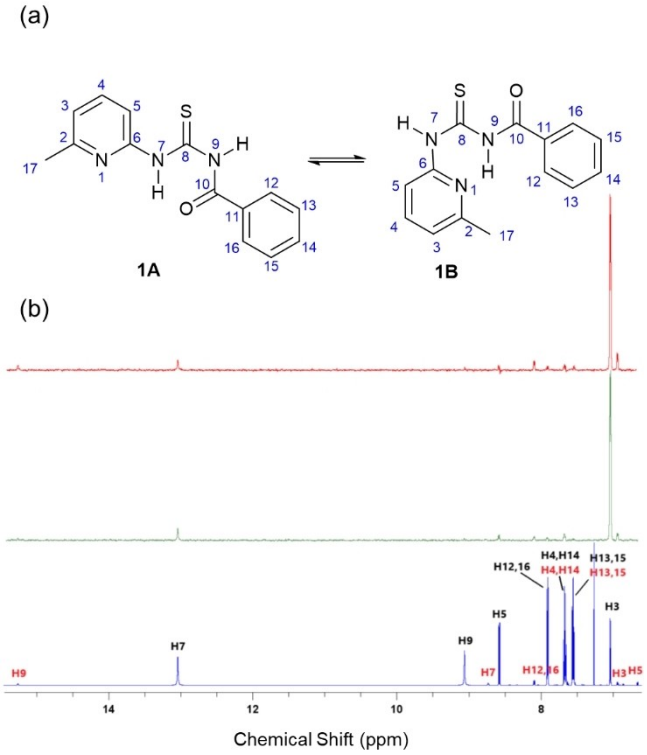

Figure 2. a) The atomic position numbering used to describe NMR resonances associated with conformers **1 A** and **1 B**; **b)** The high-frequency region of the ^{1}H NMR spectrum (in blue) and 1D NOESY spectra in $CDCl_3$ at 278 K. The methyl protons H17 of 1 A (in green) and 1B (in red) were selectively inverted in 1D NOESY experiments. Assignments of protons of **1 A** (in black) and **1 B** (in red) are also shown.

© 2024 The Authors. ChemPlusChem published by Wiley-VCH GmbH

21926506, 2024, 8, Downloaded from https://chemistry-europe.onlinelibrary.wiley.com/doi/10.1002/cplu.202400055 by Test, Wiley Online Library on [25/11/2024]. See the Terms and Conditions (https://onlinelibrary.wiley.com/terms-and-conditions) on Wiley Online Library for rules of use; OA articles are governed by the applicable Creative Commons License

changed substantially compared to $CDCl_3$ at 298 K (20.16:1 in $CDCl_3$; 10.58:1 in CD_3COCD_3; 7.28:1 in CD_3CN; 2.17:1 in DMSO-d_6). Conformer **1 A** was preferred in each case but in general the relative ratio of **1 B** increased as the polarity of the solvent increased and also correlated well with the solvent H-bond acceptor parameters β ($CHCl_3$ 0.8, nitrile 4.7, ketone 5.8, sulfoxide 8.9) reported by Hunter.[13] As in $CDCl_3$, the observed NOEs agree with linear and folded geometries of conformers **1 A** and **1 B** containing a N–H···O IHB and a N–H···N IHB respectively. The free energy of conformer **1 B** relative to **1 A** in each solvent was estimated based on the ratios in solution at 298 K (Table S10), showing that **1 B** becomes increasingly stabilised by the more polar solvent environments.

Abraham et al. have related the difference in chemical shift of an NH proton in $CDCl_3$ vs DMSO-d_6 to the hydrogen bond acidity, providing the value A_{NMR} which can be used as a quantitative assessment of intramolecular hydrogen bonding.[14] Applying this method we determined the A_{NMR} values as 0.040 (H7) and 0.364 (H9) in conformer **1 A** and 0.391 (H7) and 0.02 (H9) in conformer **1 B** (see Table S8, Supporting Information). These values suggest that strong IHBs are formed by H7 in **1 A** and by H9 in **1 B** ($A_{NMR} < 0.05$), while there are no IHBs for H9 in **1 A** and H7 in **1 B** ($A_{NMR} > 0.15$). The results also suggest that the NH···N(Py) bond in **1 B** could be stronger than the NH···O=C bond in **1 A**.

Using variable temperature (VT-NMR) experiments, the coalescence temperature was estimated to be 295 ± 2 K in DMSO-d_6 (following the methyl H17 resonances at ~2.5 ppm). We determined the free energies of activation using equations derived by Shanan-Atidi and Bar-Eli.[15] Assuming that the observed exchange is between two sites **1 A** and **1 B** with the population 2.17:1 and the chemical shift difference is 32 ± 5 Hz in the absence of the exchange (estimated from the spectrum measured at 294 K), the free energies of activation were estimated to be $\Delta G_A^{\ddagger} = 15.3 \pm 0.2$ kcal mol^{-1} (for the transition from the more populated site **1 A** to the less populated site **1 B**) and $\Delta G_B^{\ddagger} = 14.8 \pm 0.2$ kcal mol^{-1} (for the transition from the less populated site **1 B** to the more populated site **1 A**). Similarly, the coalescence temperature is 298 ± 2 K in CD_3CN for the methyl protons and assuming that the observed exchange is between two sites with the population ratio of 7.28:1 and the chemical shift difference is 35 ± 2 Hz in the absence of the exchange (measured at 238 K), the free energies of activation were $\Delta G_A^{\ddagger} = 16.0 \pm 0.2$ kcal mol^{-1} and $\Delta G_B^{\ddagger} = 14.9 \pm 0.2$ kcal mol^{-1}. The coalescence temperatures and free energies of activation under these conditions are consistent with a dynamic exchange process at room temperature, despite the expectation that 6-membered IHB rings are likely to be static.

We speculated that the addition of potential binding partners may trigger the formation of a third conformer in which both NHs could form a convergent hydrogen bonding cleft. The hydrogen bond donor units of thiourea moieties are well established as hosts for anions which can be bound through two convergent hydrogen bonds.[16] Acyl thiourea hosts have been reported to bind to basic anions such as F^- in DMSO solution.[17] Rissanen and co-workers have reported the disruption of an NH···N IHB in pyridyl ureas on titration with neutral guests containing a complimentary array of hydrogen bond donors and acceptors such as 1,8-naphthyridin-2-amine in $CDCl_3$.[18] We therefore investigated whether binding to prospective anionic guests or 1,8-naphthyridin-2-amine could trigger a conformational change in 1 to maximise potential intermolecular hydrogen bond formation to the guest. We performed ^{1}H NMR titrations with various guests in $CDCl_3$ and DMSO-d_6 (SI Section S4); however, we did not observe spectral changes that were consistent with a large conformational change. The addition of Cl^- and 1,8-naphthyridin-2-amine produced only small spectral changes (broadening of NH resonances and minimal change to other peaks), which could be consistent with weak hydrogen bond formation via a single NH. As such we concluded that the NH···O=C bond in **1 A** was unaffected by the addition of these prospective guests. Titrations with basic anions (F^-, AcO^-) produced spectral changes that were more consistent with the deprotonation of **1** rather than hydrogen bond formation (judged via comparison with an equivalent titration against *n*-tetrabutylammonium hydroxide).

Computational Conformer Screening

In order to gain insight into the structures and relative energies of **1 A** and **1 B**, we carried out an initial computational analysis in vacuo. We first performed a conformational search, identifying 45 geometries of various conformers using molecular mechanics calculations. The geometries were then optimised at the PW6B95d3/def2-TZVP level of theory, which has been shown previously to be one of the most accurate DFT methods for the characterisation of noncovalent interactions.[19] The calculated free energies of conformers were sorted with the lowest energy conformer numbered as 1 and the highest energy conformer numbered as 45 (Figure 3a and Table S9).

The lowest energy conformers 1–7 were all stabilised by a N7–H···O=C10 hydrogen bond, and so could broadly relate to conformer **1 A** identified from the NMR analysis. These are linear conformers showing small differences in relative energy (0–0.09 kcal mol^{-1}) and dihedral angles; for example, the central dihedral angle C10–N9–C8–N7 is −0.19° in conformer 1 (Figure 3b) and −0.59° in conformer 7. The π-flip of the pyridine ring about the C6–N7 bond led to conformer 8 (Figure 3b) with the free energy of 4.51 kcal mol^{-1} relative to conformer 1.

Conformers 9–16 were stabilised by a N9–H···N(Py) hydrogen bond, in line with the interaction detected in **1 B** via the NMR analysis, with relative free energies between 5.86–6.21 kcal mol^{-1}. The main difference between conformers 9 (5.86 kcal mol^{-1}) and 10 (5.90 kcal mol^{-1}) is in the sign of the dihedral angle C11–C10–N9–C8: −45.48° in 9 and 45.29° in 10. On going from conformer 9 to 11 (5.95 kcal mol^{-1}), the dihedral angle between two aromatic planes changes significantly, which can be measured as the dihedral angle C11–C10–N7–C6: 143.15° in 9 and −143.53° in 11 (Figure 3b). In conformer 12 this angle changes to −10.45° forming a fully folded geometry. The main difference between 12 and 13 is the dihedral angle C11–C10–N7–C6, which changes from −10.45° in 12 to 14.85°

© 2024 The Authors. ChemPlusChem published by Wiley-VCH GmbH

21926506, 2024, 8, Downloaded from https://chemistry-europe.onlinelibrary.wiley.com/doi/10.1002/cplu.202400055 by Test, Wiley Online Library on [25/11/2024]. See the Terms and Conditions (https://onlinelibrary.wiley.com/terms-and-conditions) on Wiley Online Library for rules of use; OA articles are governed by the applicable Creative Commons License

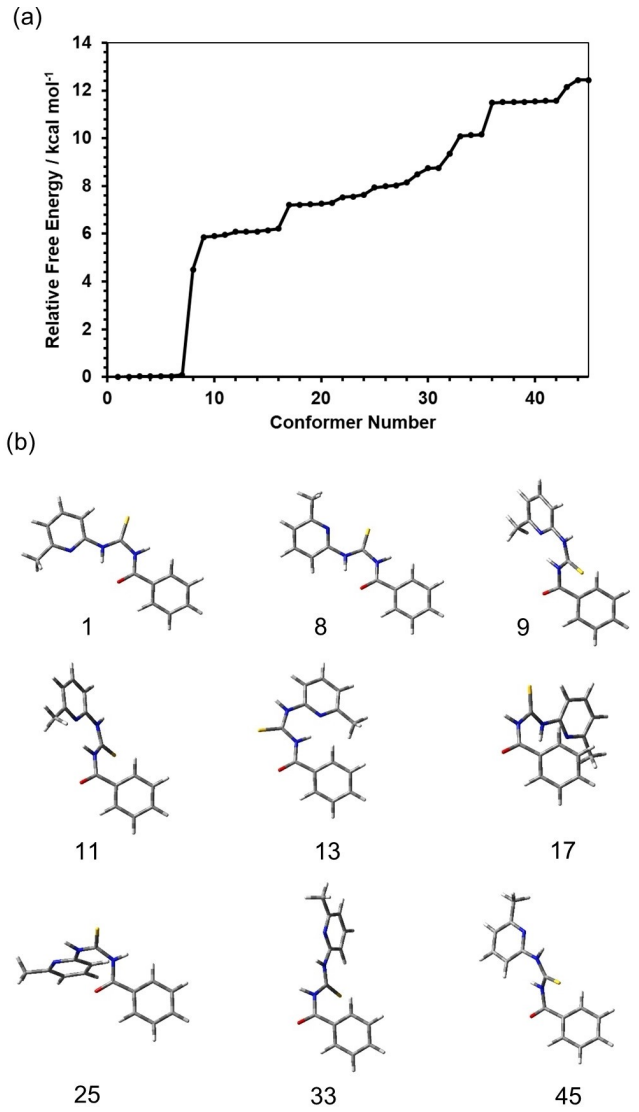

Figure 3. a) Free energies of conformers 1–45 relative to the fee energy of conformer 1; **b)** Optimised geometries of selected conformers. Calculations were performed at the PW6B95d3/def2-TZVP level of theory for a single molecule *in vacuo*.

in 13. Conformers 14–16 were similar in geometry to conformers 12 and 13. Overall, this analysis revealed that **1 A** is more stable than **1 B** in the absence of solvent and any potential intermolecular interactions.

Conformers 17–45 are significantly higher in relative free energies (7.20–12.44 kcal mol^{-1}) and do not show intramolecular hydrogen bonds. A few examples from this range are shown in Figure 3b. Conformer 33 shows a geometry, in which both NH bonds point in approximately the same direction. This is reminiscent to the possible third conformation considered above in which both NHs form a convergent hydrogen bonding cleft.[16] The DFT-predicted free energy of conformer 33 relative to that of the lowest energy conformer 1 is 9.35 kcal mol^{-1} (Figure 3a). Such a high relative energy corresponds to the population in the order of 10^{-5} %, thus suggesting that the formation of a conformation in which the two NH bonds are approximately parallel and point in the same direction is negligibly small for **1**.

Computational Analysis of Solvent Effects

In order to explore solvent polarity effects, the lowest energy conformers 1–16 were further optimised at the PW6B95d3/def2-TZVP level of theory using the SMD continuum solvation model of Truhlar et al.[20] (Figures S18 and S19 in Supporting Information). It should be noted that continuum models do not explicitly represent solvent molecules and hence explicit interactions between a solute and solvent molecules (such as potential hydrogen bonding between **1** and solvent molecules) cannot be accounted for. However, they can provide a useful approximation of solvation free energy. The results presented in Table 1 show that relative free energies of conformers in different solvents vary significantly. First, the relative free energies vary over narrower range in $CHCl_3$ (4.73 kcal mol^{-1}), CH_3CN (4.22 kcal mol^{-1}), CH_3COCH_3 (4.11 kcal mol^{-1}) and DMSO (3.65 kcal mol^{-1}) than in the gas phase (6.21 kcal mol^{-1}) and this range shrinks as the polarity of the environment increases. Remarkably, the range over which the relative free energies vary in different solvents for conformers 1–16 correlate linearly with the solvent H-bond acceptor parameter β.[13] Secondly, the relative free energy of the linear conformer 8 stabilised by the N7–H···O=C10 hydrogen bond is no longer lower than that for the folded conformer 13 stabilised by the N9–H···N(Py) hydrogen bond. Finally, the folded conformer 13 is the most preferred structure stabilised by the N9–H···N(Py) hydrogen bond in all solvents tested. The geometry of this conformer agrees with the NOEs observed in NMR experiments between the ortho- and meta-protons of the Ph ring in 1B (H12, 13, 15 and 16) and the H17 methyl protons. In particular, the nearest distances between the methyl and ortho-protons in conformer 13 are 2.83 Å ($CHCl_3$), 2.80 Å (CH_3CN) and 2.79 Å (DMSO). The corresponding distances between the methyl and meta-protons are 3.15 Å, 3.10 Å and 3.05 Å in conformer 13. For comparison, the nearest distances between the methyl and ortho-protons are 7.40–7.41 Å in conformer 1 and 5.54–5.63 Å in conformer 9 in the three solvents studied. Thus, no or negligibly small NOEs would be expected between the methyl and ortho-protons in these structures.

The lowest energy conformer containing a N9–H···N(Py) hydrogen bond is 13 (Figure 3b) in all of the solvents studied here. The relative Gibbs free energies of this form compared to the lowest energy conformer containing a N7–H···O=C10 hydrogen bond was examined using both the SMD model (Table 1) and the IEFPCM model (Table S10) to describe the solvation. These results were compared with the free energies derived from experimental NMR experiments at 298 K (Table S12). We found that both computational models qualitatively predicted the experimentally observed solvent dependence of relative free energies with some quantitative improvement in the IEFPCM model compared to the SMD model.

© 2024 The Authors. ChemPlusChem published by Wiley-VCH GmbH

21926506, 2024, 8, Downloaded from https://chemistry-europe.onlinelibrary.wiley.com/doi/10.1002/cplu.202400055 by Test, Wiley Online Library on [25/11/2024]. See the Terms and Conditions (https://onlinelibrary.wiley.com/terms-and-conditions) on Wiley Online Library for rules of use; OA articles are governed by the applicable Creative Commons License

Table 1. The calculated relative Gibbs free energies ($\Delta G°$, kcal mol^{-1}) of the lowest energy conformers 1–16 using the SMD model in $CHCl_3$, CH_3CN and DMSO. Conformers numbered in blue contain a N7–H···O=C10 hydrogen bond (as in **1 A**) and conformers numbered in red contain a N9–H···N(Py) hydrogen bond (as in **1 B**).

$CHCl_3$		CH_3COCH_3		CH_3CN		DMSO	
Conformer	ΔG°	Conformer	ΔG°	Conformer	ΔG°	Conformer	ΔG°
1	0.00	1	0.00	2	0.00	2	0.00
3	0.21	2	0.28	5	0.31	1	0.02
2	0.25	3	0.35	1	0.32	4	0.20
4	0.31	4	0.42	4	0.57	5	0.27
5	0.37	5	0.44	3	0.68	3	0.27
6	0.53	6	0.62	6	0.70	6	0.34
7	0.62	7	0.77	7	0.91	7	0.57
13	3.29	13	2.27	13	2.20	13	1.49
8	3.34	8	2.38	12	2.29	12	1.51
14	3.50	16	2.49	14	2.30	14	1.54
12	3.61	14	2.60	16	2.36	8	1.64
16	3.63	12	2.62	8	2.37	16	1.68
15	3.90	15	2.67	15	2.75	15	2.17
10	4.67	9	3.83	9	4.05	9	3.47
11	4.72	11	3.98	11	4.16	11	3.58
9	4.73	10	4.11	10	4.22	10	3.65

Interconversion Between Linear and Folded Conformers

To explore the possibility of dynamic interconversion between linear conformer 2 (containing a N7–H···O=C10 hydrogen bond) and folded conformer 13 (containing a N9–H···N(Py) hydrogen bond), we simulated rotations about the 5 single bonds joining the two aromatic rings in DMSO. The corresponding dihedral angle was either incremented or decremented in steps of 10° to simulate rotation about the selected bond. At each step, the selected dihedral angle was fixed with all of the remaining degrees of freedom optimised using PW6B95D3/def2-TZVP IEFPCM(DMSO) calculations. A relaxed 1D PES (Potential Energy Surface) scan was performed in this manner and minimised energies at each step were obtained (Supporting Information, Figures S20-S24). Maxima observed in these graphs can be considered as an energy barrier for the rotation about the bond considered. For the full 360° rotations about the bonds C11–C10, C10–N9, N9–C8, C8–N7 and N7–C6, these were 4.06, 14.87, 11.16, 18.81 and 3.22 kcal mol^{-1}, respectively. The dihedral angles in the corresponding transition states were 94, 103, 110, −61 and 184°, respectively. In order to change a conformation from linear to folded, three consecutive rotations by 180° about bonds N9–C8, C8–N7 and N7–C6 are needed, as illustrated in Figure 4a. The highest DFT-estimated barrier is about the C8–N7 bond (11.53 kcal mol^{-1}), while the overall barrier for the linear-to-folded conformer transition is 20.14 kcal mol^{-1} (Figure S27). The high energetic barrier for this rotation can be rationalised as we would expect this rotation to break the N7-H···O=C10 IHB. In principle, the value of 20.14 kcal mol^{-1} is of similar order of magnitude as the experimentally estimated free energy of activation in DMSO-d_6 ($\Delta G_A^{\ddagger} = 15.3 \pm 0.2$ kcal mol^{-1} at 294 K, see above), although it must be noted that the conditions at which these parameters are estimated are very different. Overall, these results and energetic barriers are consistent with interconversion between **1 A** and **1 B** being energetically feasible at room temperature and physiological temperatures.

A search for a transition state was also undertaken between the lowest-energy linear conformer 2 and the lowest-energy folded conformer 13 using the Synchronous Transit-guided Quasi-Newton (STQN) method[21] and the PW6B95D3/def2-TZVP IEFPCM(DMSO) level of theory via the use of optimised geometries of conformers 2 and 13 together with a "guessed" structure of the transition state in which the angle N9–C8–N7–C6 was set to −61°. A transition state was successfully identified, showing only one imaginary frequency, but its free energy relative to conformer 2 was only 2.97 kcal mol^{-1}. Further analysis revealed this low energy transition state to be associated with the rotation of the pyridyl methyl group. We then considered model structures of conformers 2 and 13 (denoted as 2b and 13b) and the transition state (denoted TS-2b-13b) in which the methyl group was replaced by a hydrogen atom. The transition state identified in this manner (shown in Figure 4b) together with conformers 2b and 13b had a free energy of 18.77 kcal mol^{-1} and 16.85 kcal mol^{-1} relative to conformers 2b and 13b, respectively, which are in satisfactory agreement with experimental NMR measurements and the PES analysis considered above.

Finally, we considered whether conformational switching may impact the drug-like properties of compound **1**. Firstly, we assessed whether a change of conformation was likely on moving from the blood to the hydrophobic interior of a cell

© 2024 The Authors. ChemPlusChem published by Wiley-VCH GmbH

21926506, 2024, 8, Downloaded from https://chemistry-europe.onlinelibrary.wiley.com/doi/10.1002/cplu.202400055 by Test, Wiley Online Library on [25/11/2024]. See the Terms and Conditions (https://onlinelibrary.wiley.com/terms-and-conditions) on Wiley Online Library for rules of use; OA articles are governed by the applicable Creative Commons License

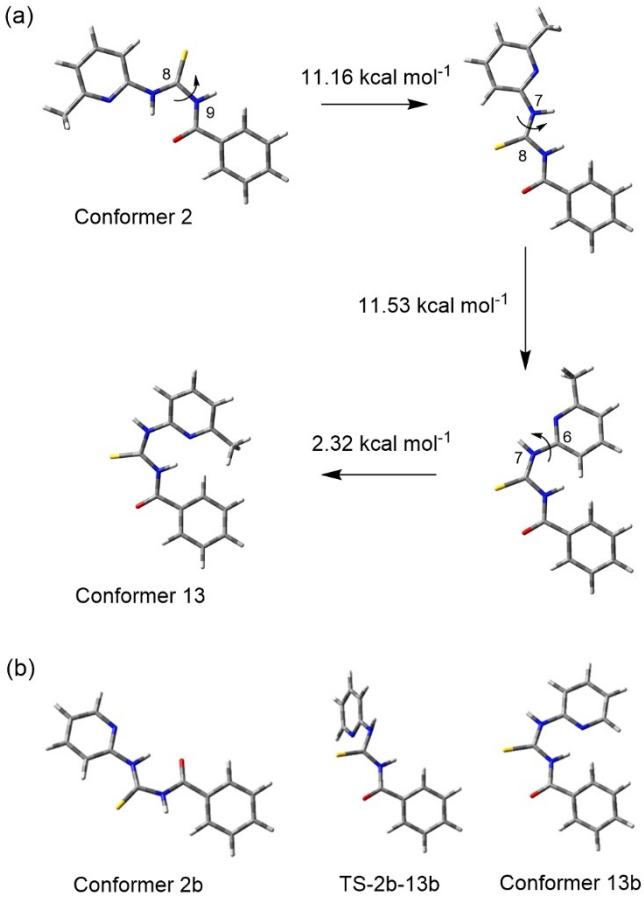

Figure 4. a) Schematic representation of the transition from a linear conformer 2 (top left) to a folded conformer 13 (bottom left) via three π-flips about bonds N9–C8, C8–N7 and N7–C6. The DFT-estimated energetic barrier for each rotation is given next to the arrows (see Figures S22, S25 and S26); b) Geometries of conformers 2b and 13b optimised at the PW6B95D3/def2-TZVP IEFPCM(DMSO) level of theory. The transition state (TS-2b–13b) associated with the C8–N7 bond rotation is also shown. The dihedral angle N9–C8–N7–C6 was 179.36° in 2b, 118.50° in TS-2b-13b and −0.64° in 13b. The two N–H bond directions are perpendicular in the transition state, forming a dihedral angle of −90.5° (H–N7∧N9–H). This angle is 173.82° in 2b and −178.14° in 13b.

membrane by calculating the relative Gibbs free energy of the various low-energy conformers in water and in n-hexane using the IEFPCM model (Table S11). The lowest energy linear conformer containing a N7–H···O=C10 hydrogen bond was conformer 2 in water and conformer 1 in *n*-hexane, while the lowest energy folded conformer containing a N9–H···N(Py) hydrogen bond was conformer 12 in water and conformer 15 in *n*-hexane. Similar to the results of the calculations in other solvents, the energy of the minor folded conformer (shown in bold in Tables S10 and S11) relative to that of the unfolded conformer decreases gradually, from 4.42 to 1.47 kcal mol^{-1}; thus the proportion of each conformer would be expected to vary drastically on moving between the blood and a cell membrane.

We also calculated the solvent accessible 3D polar surface area (3D PSA) of representative calculated structures of conformers **1 A** and **1 B** using PyMOL according to a method reported by Matsson and Kihlberg.[4c] The results, shown in Table S13 revealed that **1 B** has a slightly larger 3D PSA than **1 A**, which correlates with the finding that **1 B** is increasingly favoured by polar solvent environments. However, the difference is relatively small (4.653 Å^2) due to the small molecular size of **1** and the limited number of hydrogen bond donors and acceptors.

X-ray Crystallography

An X-ray crystal structure of compound **1** has been previously reported, in which the molecule adopts a **1 B** conformation (containing a N9–H···N(Py) hydrogen bond). We screened a variety of crystallisation conditions to obtain single crystals of compound **1** in different conformations. Interestingly, the previously reported solid-state conformer was obtained preferentially in the majority of the crystallisations we attempted. The single crystal X-ray structure of one such crystal (grown by slow evaporation of a solution of **1** in acetonitrile) is shown in Figure 5. We also obtained single crystals of a **1 A** conformation (containing a N7–H···O=C10 hydrogen bond) by slow evaporation of a solution of **1** in acetone and acetone/water (9:1),

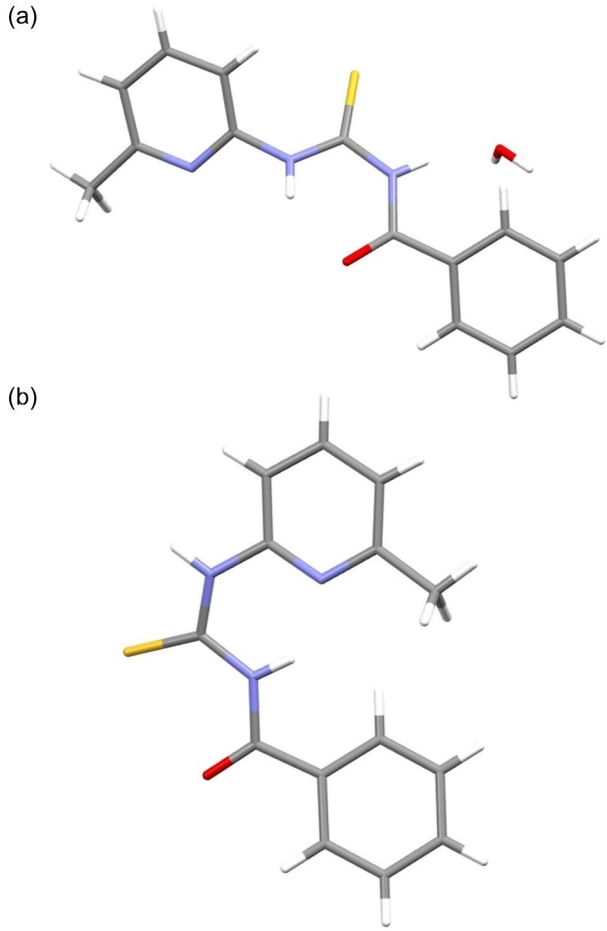

Figure 5. Single crystal X-ray structures of (a) **1 A** and (b) **1 B**. Colour scheme: carbon – grey, hydrogen – white, nitrogen – blue, oxygen – red, sulfur – yellow.

© 2024 The Authors. ChemPlusChem published by Wiley-VCH GmbH

21926506, 2024, 8, Downloaded from https://chemistry-europe.onlinelibrary.wiley.com/doi/10.1002/cplu.202400055 by Test, Wiley Online Library on [25/11/2024]. See the Terms and Conditions (https://onlinelibrary.wiley.com/terms-and-conditions) on Wiley Online Library for rules of use; OA articles are governed by the applicable Creative Commons License

and the resulting structure is shown in Figure 5. The crystallisation behaviour of **1 A** was erratic and at times we experienced reproducibility issues in obtaining crystals of this solid-state conformer.[22] Full details of the crystallographic studies can be found in the SI Section S5.

The crystal structure of **1 A** shows a conformation which is similar to the lowest energy conformers 1–7 identified in the computational analysis. The central dihedral angle C10–N9–C8–N7 in the X-ray structure is 11.83 °, showing some deviation from planarity within the 6-membered intramolecular hydrogen bonding ring. In this case, the structure obtained was a hydrate with one water molecule associated to N7–H. The N7···OH_2 distance is 2.988 Å indicating a moderate, mostly electrostatic interaction.[23] The crystal structure of **1 B** shows a fully folded conformer with a dihedral angle between two aromatic planes C11–C10ΛN7–C6 of 0.18°. This arrangement is comparable to the folded conformation observed in conformers 12–16 in the computational analysis. The 6-membered intramolecular hydrogen bonding ring deviates from planarity, with an N9–C8–N7–C6 angle of 10.61°. One explanation for the preferred crystallisation of **1 B** over **1 A** may be the formation of pi-stacking interactions in the structure of **1 B** which are absent in the structure we obtained for **1 A** (see SI Figure S26). Additionally, the structure we obtained of **1 A** was a hydrate, containing bridging water molecules; thus, the water content of the crystallisation solvent may have played a significant role in determining the outcome and could explain why this structure was rarely obtained

Conclusions

In conclusion, we have studied the conformational preferences of a molecule with a choice of two 6-membered IHB interactions. Compound **1** displays solvent-polarity dependent conformational preferences. NMR and DFT results suggest that interconversion between low energy conformers is dynamic under the conditions used here, contradicting expectations based on Kuhn's topologies that 6-membered pseudorings are likely to be static. Considering the host of biological and medicinal applications reported for acyl thiourea targets,[11,24] we hope that this work can help understanding of the static/dynamic nature of the IHB in this motif and shed light on their pharmacokinetic properties. More broadly, this work presents a new strategy to design targets with dynamic IHBs by introducing competitive IHB pathways. This could guide the identification and design of new molecular chameleons and further the development of drug candidates in bRo5 chemical space.

Supporting Information

The authors have cited additional references within the Supporting Information.[4c,12,14,20,25] The Supporting Information includes information relating to the synthesis of **1**, NMR analysis, computational modelling, NMR titrations and crystal structure analysis.

Deposition Numbers 2302287 (for 1A), 2302286 (for 1B), contain the supplementary crystallographic data for this paper. These data are provided free of charge by the joint Cambridge Crystallographic Data Centre and Fachinformationszentrum Karlsruhe Access Structures service.

Acknowledgements

CJEH thanks University College London for financial support for Master's students (YS, HB, V. B.-M.) and a PhD studentship (ERM).

Conflict of Interests

The authors declare no conflict of interest.

Data Availability Statement

The data that support the findings of this study are available in the supplementary material of this article.

Keywords: intramolecular hydrogen bonding · conformational analysis · drug design · NMR · dynamic exchange

[1] a) G. Caron, J. Kihlberg, G. Ermondi, *Med. Res. Rev.* **2019**, *39*, 1707–1729; b) B. Kuhn, P. Mohr, M. Stahl, *J. Med. Chem.* **2010**, *53*, 2601–2611.
[2] S. Sasaki, N. Cho, Y. Nara, M. Harada, S. Endo, N. Suzuki, S. Furuya, M. Fujino, *J. Med. Chem.* **2003**, *46*, 113–124.
[3] V. A. Ashwood, M. J. Field, D. C. Horwell, C. Julien-Larose, R. A. Lewthwaite, S. McCleary, M. C. Pritchard, J. Raphy, L. Singh, *J. Med. Chem.* **2001**, *44*, 2276–2285.
[4] a) A. Alex, D. S. Millan, M. Perez, F. Wakenhut, G. A. Whitlock, *MedChemComm* **2011**, *2*, 669–674; b) P. Matsson, B. C. Doak, B. Over, J. Kihlberg, *Adv. Drug Delivery Rev.* **2016**, *101*, 42–61; c) M. Rossi Sebastiano, B. C. Doak, M. Backlund, V. Poongavanam, B. Over, G. Ermondi, G. Caron, P. Matsson, J. Kihlberg, *J. Med. Chem.* **2018**, *61*, 4189–4202; d) L. H. E. Wieske, Y. Atilaw, V. Poongavanam, M. Erdélyi, J. Kihlberg, *Chem. Eur. J.* **2023**, *29*, e202202798; e) G. Caron, J. Kihlberg, G. Goetz, E. Ratkova, V. Poongavanam, G. Ermondi, *ACS Med. Chem. Lett.* **2021**, *12*, 13–23.
[5] M. Tyagi, V. Poongavanam, M. Lindhagen, A. Pettersen, P. Sjö, S. Schiesser, J. Kihlberg, *Org. Lett.* **2018**, *20*, 5737–5742.
[6] a) C. J. E. Haynes, N. Busschaert, I. L. Kirby, J. Herniman, M. E. Light, N. J. Wells, I. Marques, V. Felix, P. A. Gale, *Org. Biomol. Chem.* **2014**, *12*, 62–72; b) E. Contreras Aguilar, G. A. Echeverría, O. E. Piro, S. E. Ulic, J. L. Jios, M. E. Tuttolomondo, R. D. I. Molina, M. E. Arena, *Chem. Phys. Lett.* **2019**, *715*, 64–71.
[7] J.-L. Vidaluc, F. Calmel, D. Bigg, E. Carilla, A. Stenger, P. Chopin, M. Briley, *J. Med. Chem.* **1994**, *37*, 689–695.
[8] G. R. Desiraju, *J. Am. Chem. Soc.* **2013**, *135*, 9952–9967.
[9] E. Parisi, et al., *Dalton Trans.* **2020**, *49*, 14452–14462.
[10] S. Fusco, E. Parisi, A. Carella, A. Capobianco, A. Peluso, C. Manfredi, F. Borbone, R. Centore, *Cryst. Growth Des.* **2018**, *18*, 6293–6301.
[11] a) T. Chia, T. Nakamura, M. Amano, N. Takamune, M. Matsuoka, H. Nakata, *Antimicrob. Agents Chemother.* **2021**, *65*, 10.1128/aac.01039-01021; b) T. Kobayakawa, et al., *RSC Med. Chem.* **2023**, *14*, 1973–1980.
[12] F. Adhami, M. Safavi, M. Ehsani, S. K. Ardestani, F. Emmerling, F. Simyari, *Dalton Trans.* **2014**, *43*, 7945–7957.
[13] C. A. Hunter, *Angew. Chem. Int. Ed.* **2004**, *43*, 5310–5324.
[14] M. H. Abraham, R. J. Abraham, W. E. Acree Jr., A. E. Aliev, A. J. Leo, W. L. Whaley, *J. Org. Chem.* **2014**, *79*, 11075–11083.
[15] H. Shanan-Atidi, K. H. Bar-Eli, *J. Phys. Chem.* **1970**, *74*, 961–963.

© 2024 The Authors. ChemPlusChem published by Wiley-VCH GmbH

21926506, 2024, 8, Downloaded from https://chemistry-europe.onlinelibrary.wiley.com/doi/10.1002/cplu.202400055 by Test, Wiley Online Library on [25/11/2024]. See the Terms and Conditions (https://onlinelibrary.wiley.com/terms-and-conditions) on Wiley Online Library for rules of use; OA articles are governed by the applicable Creative Commons License

[16] A.-F. Li, J.-H. Wang, F. Wang, Y.-B. Jiang, *Chem. Soc. Rev.* **2010**, *39*, 3729–3745.
[17] S. Hu, Y. Guo, J. Xu, S. Shao, *Spectrochim. Acta Part A* **2009**, *72*, 1043–1046.
[18] B. Ośmiałowski, K. Mroczyńska, E. Kolehmainen, M. Kowalska, A. Valkonen, M. Pietrzak, K. Rissanen, *J. Org. Chem.* **2013**, *78*, 7582–7593.
[19] L. Nunar, A. E. Aliev, *Chem. Methods* **2023**, *3*, e202200044.
[20] A. V. Marenich, C. J. Cramer, D. G. Truhlar, *J. Phys. Chem. B* **2009**, *113*, 6378–6396.
[21] C. Peng, H. Bernhard Schlegel, *Isr. J. Chem.* **1993**, *33*, 449–454.
[22] a) J. D. Dunitz, J. Bernstein, *Acc. Chem. Res.* **1995**, *28*, 193–200; b) D.-K. Bučar, R. W. Lancaster, J. Bernstein, *Angew. Chem. Int. Ed.* **2015**, *54*, 6972–6993.
[23] J. J. Dannenberg, *J. Am. Chem. Soc.* **1998**, *120*, 5604–5604.
[24] a) S. Cunha, F. C. Macedo, G. A. N. Costa, M. T. Rodrigues, R. B. V. Verde, L. C. de Souza Neta, I. Vencato, C. Lariucci, F. P. Sá, *Monatsh. Chem.* **2007**, *138*, 511–516; b) D. L. Wyles, K. A. Kaihara, R. T. Schooley, *Antimicrob. Agents Chemother.* **2008**, *52*, 1862–1864; c) K. Sambanthamoorthy, R. E. Sloup, V. Parashar, J. M. Smith, E. E. Kim, M. F. Semmelhack, M. B. Neiditch, C. M. Waters, *Antimicrob. Agents Chemother.* **2012**, *56*, 5202–5211; d) T. O. Brito, A. X. Souza, Y. C. C. Mota, V. S. S. Morais, L. T. de Souza, Â. de Fátima, F. Macedo, L. V. Modolo, *RSC Adv.* **2015**, *5*, 44507–44515; e) M. K. Rauf, A. Talib, A. Badshah, S. Zaib, K. Shoaib, M. Shahid, U. Flörke, D. Imtiaz ud, J. Iqbal, *Eur. J. Med. Chem.* **2013**, *70*, 487–496.
[25] a) H. E. Gottlieb, V. Kotlyar, A. Nudelman, *J. Org. Chem.* **1997**, *62*, 7512–7515; b) G. R. Fulmer, A. J. M. Miller, N. H. Sherden, H. E. Gottlieb, A. Nudelman, B. M. Stoltz, J. E. Bercaw, K. I. Goldberg, *Organometallics* **2010**, *29*, 2176–2179; c) D. Neuhaus, M. P. Williamson, *The Nuclear Overhauser Effect in Structural and Conformational Analysis*, 2nd ed., Wiley-VCH, New York, **2000**; d) M. F. Schlecht, *Molecular Modeling on the PC*. Wiley-VCH, New York, **1998**. Software used: PCMODEL (version 8.5, Serena Software); e) Avogadro: an open-source molecular builder and visualization tool. Version 1.93. http://avogadro.cc/; f) M. D. Hanwell, D. E. Curtis, D. C. Lonie, T. Vandermeersch, E. Zurek, G. R. Hutchison, *J. Cheminf.* **2012**, *4*, 17; g) GaussView, Version 6.1.1, R. Dennington, T. Keith,, J. Millam, Semichem Inc., Shawnee Mission, KS, **2019**; h) Gaussian 16, Revision C.01, M. J. Frisch, G. W. Trucks, H. B. Schlegel, G. E. Scuseria, M. A. Robb, J. R. Cheeseman, G. Scalmani, V. Barone, G. A. Petersson, H. Nakatsuji, X. Li, M. Caricato, A. V. Marenich, J. Bloino, B. G. Janesko, R. Gomperts, B. Mennucci, H. P. Hratchian, J. V. Ortiz, A. F. Izmaylov, J. L. Sonnenberg, D. Williams-Young, F. Ding, F. Lipparini, F. Egidi, J. Goings, B. Peng, A. Petrone, T. Henderson, D. Ranasinghe, V. G. Zakrzewski, J. Gao, N. Rega, G. Zheng, W. Liang, M. Hada, M. Ehara, K. Toyota, R. Fukuda, J. Hasegawa, M. Ishida, T. Nakajima, Y. Honda, O. Kitao, H. Nakai, T. Vreven, K. Throssell, J. A. Montgomery, Jr., J. E. Peralta, F. Ogliaro, M. J. Bearpark, J. J. Heyd, E. N. Brothers, K. N. Kudin, V. N. Staroverov, T. A. Keith, R. Kobayashi, J. Normand, K. Raghavachari, A. P. Rendell, J. C. Burant, S. S. Iyengar, J. Tomasi, M. Cossi, J. M. Millam, M. Klene, C. Adamo, R. Cammi, J. W. Ochterski, R. L. Martin, K. Morokuma, O. Farkas, J. B. Foresman, D. J. Fox, Gaussian, Inc., Wallingford CT, 2019; i) Y. Zhao, D. G. Truhlar, *J. Phys. Chem. A.* **2005**, *109*, 5656–5667; j) F. Weigend, R. Ahlrichs, *Phys. Chem. Chem. Phys.* **2005**, *7*, 3297–3305; k) F. Weigend, *Phys. Chem. Chem. Phys.* **2006**, *8*, 1057–1065; l) I. M. Alecu, J. Zheng, Y. Zhao, D. G. Truhlar, *J. Chem. Theory Comput.* **2010**, *6*, 2872–2887; m) E. Cancès, B. Mennucci, *J. Math. Chem.* **1998**, *23*, 309–326; n) M. Cossi, N. Rega, G. Scalmani, V. Barone, *J. Comput. Chem.* **2003**, *24*, 669–681; o) https://gaussian.com/scrf/; p) CrysAllisPro, Agilent Technologies Inc., **2022**; q) G. Sheldrick, *Acta Crystallogr. Sect. C* **2015**, *71*, 3–8; r) O. V. Dolomanov, L. J. Bourhis, R. J. Gildea, J. A. K. Howard, H. Puschmann, *J. Appl. Crystallogr.* **2009**, *42*, 339–341; s) G. M. Sheldrick, *Acta Crystallogr. Sect. A* **2015**, *71*, 3–8.

Manuscript received: January 22, 2024
Revised manuscript received: April 30, 2024
Accepted manuscript online: May 7, 2024
Version of record online: June 4, 2024

© 2024 The Authors. ChemPlusChem published by Wiley-VCH GmbH

21926506, 2024, 8, Downloaded from https://chemistry-europe.onlinelibrary.wiley.com/doi/10.1002/cplu.202400055 by Test, Wiley Online Library on [25/11/2024]. See the Terms and Conditions (https://onlinelibrary.wiley.com/terms-and-conditions) on Wiley Online Library for rules of use; OA articles are governed by the applicable Creative Commons License